J Mater Sci (2010) 45:3858–3865
DOI 10.1007/s10853-010-4441-4

Poly(anthranilic acid)/multi-walled carbon nanotube composites: spectral, morphological, and electrical properties

Matru Prasad Dash · Minaketan Tripathy · Abhisek Sasmal · Gourang C. Mohanty · P. L. Nayak

Received: 21 January 2010 / Accepted: 22 March 2010 / Published online: 7 April 2010

Abstract In this research article, we have described the synthesis of acid (HCl)-doped poly(anthranilic acid) (PAA) with carboxylic groups containing multi-walled carbon nanotubes (c-MWNTs) via in situ polymerization. Anthranilic acid monomers were adsorbed on the surface of MWNTs and polymerized to form PAA/c-MWNT composites. The structure of PAA/c-MWNT composites was characterized by UV–vis spectra, Fourier transform infrared spectroscopy, nuclear magnetic resonance, and X-ray diffraction patterns. Scanning electron microscopy and transmission electron microscopy images showed that both the thinner fibrous phase and the larger block phase could be observed. The individual fibrous phases had diameters of about 100 nm, and therefore, must be the carbon nanotubes (diameter 10–20 nm) coated by a PAA layer. The electrical conductivities of PAA/c-MWNT increased with the increase of c-MWNT content.

Introduction

Since the discovery of carbon nanotubes (CNT) in 1991 by Iijima [1], they have been considered as ideal reinforcing fillers in nanocomposite materials. Some key properties include high mechanical strength, high aspect ratio, small diameter, light weight, high electrical and thermal conductivities, and high thermal and air stabilities [2–13]. They have the potential to be used in areas such as field emitters [14], probe tips for SPMs [15], nanoelectronic devices [16, 17], and nanotube-based composites [10, 18]. In recent years, considerable research has been undertaken on the preparation of novel nanocomposites with CNTs as fillers in composite materials. A wide range of host materials have been used, including polymers, ceramics, and metals [19–22]. Several methods have been developed to prepare these polymer/CNT composites, such as melt mixing [20], in situ polymerization [23], mini-emulsion polymerization [24], electrochemical [25], electrospinning [26, 27], and other methods [28, 29]. Among these polymer/CNT composites, conducting polymers/CNT composites, including poly (*p*-phenylenevenylene) (PPV)/CNT, poly(3-octylthiophene)/CNT, and poly(3,4-ethylenedioxythiophene) (PEDOT)/CNT, have received great attention because of their unique electrical properties as well as extensive application in photovoltaic cells and organic light-emitting diodes [30–32].

Among the various conducting polymers, polyaniline (PANI) has potential uses in synthesizing polymer/CNT composites owing to its good processibility, environmental stability, and its oxidation or protonation-adjustable electro-optical properties [33, 34].Considerable advancement has been made in designing and fabricating some PANI/CNT composites due to their unique electrical properties as well as extensive application in electronic devices [35–37]. Recently, many new methods to synthesize PANI/CNT composites have been well studied by several groups. Wan and co-workers [38] have synthesized PANI nanotubes doped with sulfonated CNTs via a self-assembly process. Maser and co-workers [39] reported the formation of a soluble self-aligned PANI/CNT films by a simple in situ

M. P. Dash · A. Sasmal · P. L. Nayak (✉)
P.L. Nayak Research Foundation, Post-C.R.R.I., Cuttack 753006, India
e-mail: plnayak@rediffmail.com

M. Tripathy
Faculty of Pharmacy, U.I.T.M., Mara, Malaysia

G. C. Mohanty
Department of Physics, Ravenshaw University, Cuttack 753003, India

method. Zhang and co-workers [35] developed a cationic surfactant-directed method to synthesize PANI/CNT nanocable composites. Wu et al. [40] obtained tubular PANI/CNT composites by in situ polymerization from carboxylic group-capped CNTs. However, the major disadvantage of PANI/CNT is its insolubility in common organic solvents and its infusibility. Hence, there is a search to find out water soluble PANI derivative to be reacted with MWNT for greater solubility and better processibility.

In this research study, ortho carboxyl-substituted aniline, anthranilic acid, has been chosen to be polymerized with MWNT. Anthranilic acid (*o*-amino benzoic acid) is a good candidate to be polymerized with MWNT. Poly(anthranilic acid) (PAA) seemed to be a promising material due to its high processibility, the presence of a redox-active substituent, and the ability to self-dope, all these characteristics attributable to the carboxylic acid group. PAA is much more soluble than its parent polymer. PAA exhibits solubility in a range of solvents, including basic aqueous solution [41], alcohols, and other polar solvents [42]. The carboxylic acid group can be reduced and oxidized; this may provide an additional mode of charge storage (pseudo capacitance) for the super capacitor. Self-doping has the advantage of being a faster doping process than the one seen in externally doped polyanilines, where the dopant ion must move in and out of the polymer chain [43]. It has been reported that PAA itself is not electro-active, but that a copolymer of aniline and anthranilic acid may be [44]. The four oxidation states of PAA are presented in Fig. 1.

In the present communication, we have described the synthesis and characterization of PAA with MWNT fabricated by in situ polymerization. The nanocomposites were characterized by a number of techniques including ultraviolet (UV)–visible, Fourier transform infrared spectroscopy (FTIR), nuclear magnetic resonance (NMR), scanning electron microscopy (SEM), transmission electron microscopy (TEM), X-ray diffraction (XRD), and electrical conductivity.

Work-up procedure

Materials

Anthranilic acid and aniline monomers were purchased from Aldrich. Multi-walled CNT (>90% purification) used in this study was purchased from Cheap Tubes (USA, 10–20 nm diameter). Other reagents like ammonium persulfate (APS), hydrochloric, sulfuric, and nitric acid (Sigma Chemicals) were of analytical grade.

Oxidation of MWNT

MWNTs were suspended in a 3:1 mixture of concentrated H_2SO_4 and HNO_3 and refluxed for 30 min in an ultrasonic bath. The solution was magnetically stirred and heated at 60 °C for 24 h. This treatment provides carboxylic acid groups at defects in the surface of tubes and exfoliates graphite. The obtained c-MWNTs were filtered through 0.2-μm polytetrafluoroethylene (PTFE) membrane filter, washed with plenty of deionized water until the pH value was around 7, and then dried at 70 °C for 24 h.

Synthesis of PAA/c-MWNT polymer composites

PAA/c-MWNT composites were synthesized by in situ chemical oxidative polymerization of PAA. In a typical experiment, various weight ratios of c-MWNTs were

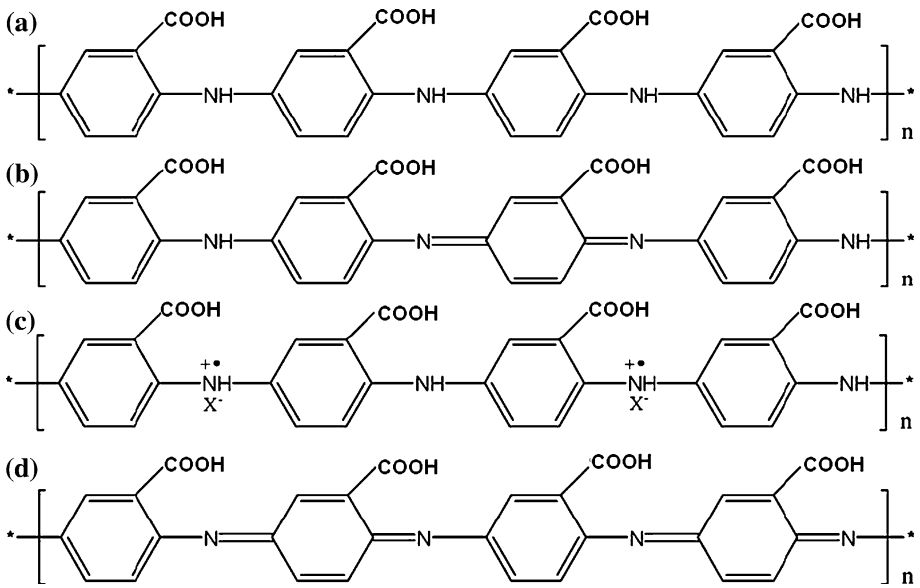

Fig. 1 Four different redox forms of PAA: **a** leucoemeraldine base (fully reduced form), **b** emeraldine base (half-oxidized form), **c** conducting emeraldine salt (half-oxidized and protonated form), and **d** pernigraniline base (fully oxidized form)

dissolved in 80 mL 1.2 M hydrochloric acid solutions and ultrasonicated over 2 h, transferred into a 250-mL beaker, aniline (0.20 g, 15% of anthranilic acid), and anthranilic acid (1.37 g) were added to the above c-MWNT suspension [45]. Subsequently, 50 mL of a 1.2 M HCl solution containing 6.8 g of APS was added into the suspension with constant mechanical stirring at room temperature. The reaction mixture was stirred for a further 12 h, and then filtered. The remaining filter cake was rinsed several times with distilled water and ethanol. The powder thus obtained was dried under vacuum at 60 °C for 24 h. The % of c-MWNT used was 0, 2, 5, and 10%.

Measurement

UV–vis absorption spectra measurement

For the absorbance measurements, the solids (in the untreated, as obtained, form) were dissolved in *N*-methylpyrrolidone (NMP), and the UV–vis spectra were recorded in the range 300–1,000 nm. Then, hydrochloric acid was added to reduce the (co)polymer, and the absorption spectra were recorded again. All the UV–vis measurements were performed using a Shimadzu PC3101 spectrophotometer, under computer control.

IR spectra

The Fourier transform infrared (FT-IR) spectra were recorded on a Nicolet 8700 spectrometer, in the range 400–4,000 cm^{-1}.

NMR

^{1}H NMR measurements were carried out using a Bruker Avance II 500 MHz multinuclear spectrometer. The spectra were analyzed with the aid of simulations using two different simulators.

Morphology

Morphology of the PAA/c-MWNTS composite was investigated using a Philip XL 30 SEM at an accelerating voltage of 25 kV. The sample was fractured at liquid nitrogen temperature and then was coated with a thin layer of gold before observation.

TEM

TEM experiments were performed on a Hitachi H-8100 electron microscope with an acceleration voltage of 200 kV.

XRD

X-ray diffraction (Rigaku, D/Max, 2,500 V, Cu-Kα radiation: 1.54056 Å) experiments were carried out on both the plain PAA and the composite samples. Wide-angle X-ray diffractograms were recorded at temperature of 30 °C after isothermal crystallization at this temperature for 1 h in the range of 0–80 (2θ).

Conductivity

The standard Van Der Pauw DC four-probe method was used to measure the electron transport behaviors of PAA and PAA/c-MWNT composites. The samples of PAA and PAA/c-MWNTs were pressed into pellet. The pellet was cut into a square. The square was placed on the four probe apparatus, providing a voltage for the corresponding electrical current could be obtained. The electrical conductivity of samples was calculated by the following formula: σ (S/cm) = (2.44 × 10/*S*) × (*I*/*E*), where σ is the conductivity, *S* the sample side area, *I* the current passed through outer probes, and *E* the voltage drop across inner probes.

Results and discussion

UV

The UV–vis spectra of the PAA/c-MWNTs in NMP solutions are presented in Fig. 2. Owing to deprotonation effects of NMP, the spectra are similar to those of emeraldine base of PAA. The major peak at 316 and 618 nm are assigned to the excitation of the benzene and quinoid segments on the polyemeraldine chain, respectively. In order to obtain the doped PAA/c-MWNTs, one drop of

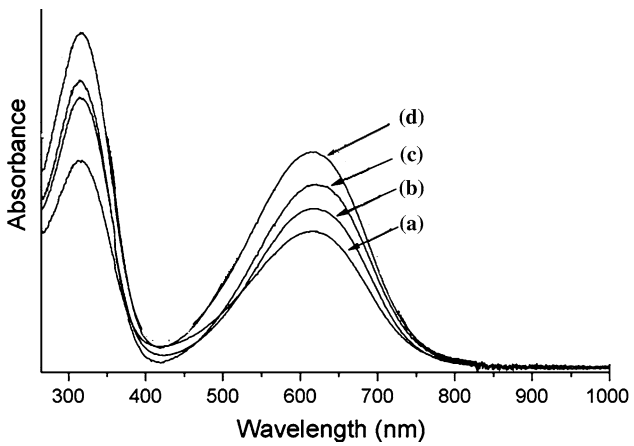

Fig. 2 UV–vis spectra of PAA/c-MWNT composites in NMP solutions: *a* 0 wt% c-MWNTs; *b* 2 wt% c-MWNTs; *c* 5 wt% c-MWNTs; *d* 10 wt% c-MWNTs

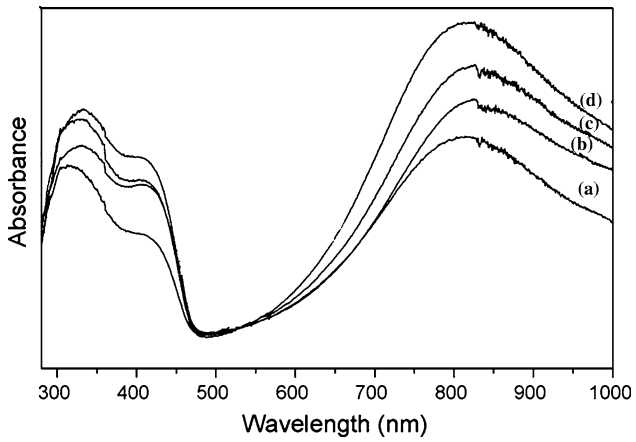

Fig. 3 UV–vis spectra of PAA/c-MWNT composites in NMP solutions after adding one drop of 35% HCl solution: *a* 0 wt% c-MWNTs; *b* 2 wt% c-MWNTs; *c* 5 wt% c-MWNTs; *d* 10 wt% c-MWNTs

35 wt% HCl is added to the above solutions. The absorption peaks at 320, 410, and 820 nm are presented in Fig. 3. The absorption peak at about 320 nm can be attributed to π–π^* transition of the benzenoid rings, whereas the peaks at around 410 and 820 nm can be attributed to polaron–π^* and π–polaron transition, respectively.

FT-IR of c-MWNT

The surface functionalization of MWNTs has usually been accomplished by introducing carboxylic acid moieties onto their surfaces. Carboxylic acid functionalization was confirmed by FT-IR spectrum shown in Fig. 4. The bands at around 3,350 and 1,200 cm^{-1} are attributed to the presence of hydroxyl groups (–OH) on the surface of MWNTs, which could appear either from ambient moisture bound to the MWNTs or during the purification of raw material [46]. The presence of carboxylic acid groups on c-MWNTs was confirmed with a C=O band stretching that appears at around 1,740 cm^{-1}, whereas the band at 1,250 cm^{-1} is attributed to the C–O stretching vibrations of –COOH groups. These observations clearly indicate the existence of –COOH groups on the surface of MWNTs.

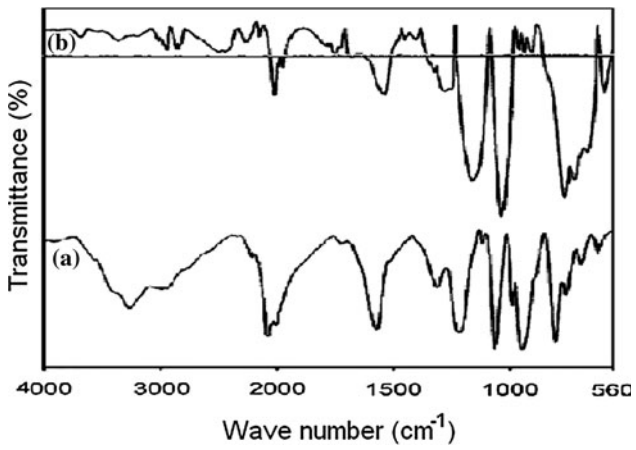

Fig. 4 FT-IR spectra of *a* pristine and *b* acid functionalized MWCNTs

FT-IR spectra of PAA/C-MWNT

The FT-IR spectra used to characterize the structure of PAA/c-MWNT composites are presented in Fig. 5. The FTIR spectrum for PAA shows strong bands for the C=O stretching at 1,681 cm^{-1} and C–N stretching at 1,132 cm^{-1}. The absorption at 1,497 cm^{-1} is due to the –N–H– stretching vibration. The vibration modes of the benzene rings appear between 1,570 cm^{-1}. In addition, the band appearing at 756 cm^{-1} probably corresponds to the C–H out-of-plane bending vibration of the 1,2,3-trisubstituted benzene rings. The presence of carboxylic acid groups was confirmed with a C=O band stretching that appears around 1,681 cm^{-1}, whereas the band at 1,249 cm^{-1} is attributed to the C–O stretching vibrations of –COOH groups. The absorption at 1,570 cm^{-1} is due to the C=C stretching in benzene ring. In addition, the band appearing at 758 cm^{-1} corresponds to the C–H out-of-plane bending vibration of the 1,2,3-trisubstituted benzene rings.

NMR spectra

The proton NMR spectra of PAA and c-MWNT/PAA are shown in the Fig. 6. The spectrum of PAA shows signals 7.3–7.8 ppm is due to protons on the aromatic ring of PAA. Further the interaction between PAA and c-MWNT for all the samples show the proton signal in the range 7.3–7.8 ppm. The broadened ^1H NMR signal of the polymer-wrapped c-MWNT may be attributed to homogeneities in the local magnetic field.

SEM

The SEM pictures of the pristine MWNTs, c-MWNTs, bare copolymer, and nanocomposite with 2, 5, and 10% c-MWNTs are presented in Fig. 7. The pristine c-MWNT morphology is displayed in Fig. 8a as endless, tangled, hollow ropes with a smooth surface, and the diameter of each nanotube is about 10–20 nm. Figure 8b shows the disentanglement of the c-MWNTs, and the slight reduction in the length of the nanotubes is observed after oxidation with 3:1 concentrated H_2SO_4 and HNO_3 mixture. It is clear from Fig. 8c that the bulk copolymer synthesized without c-MWNTs shows a typical morphology. In the case of nanocomposite (Fig. 8d), a tubular layer of coated copolymer film is clearly present on the surface of c-MWNTs, and the diameter of the nanocomposite is increased substantially as compared to that of the c-MWNTs, depending on the

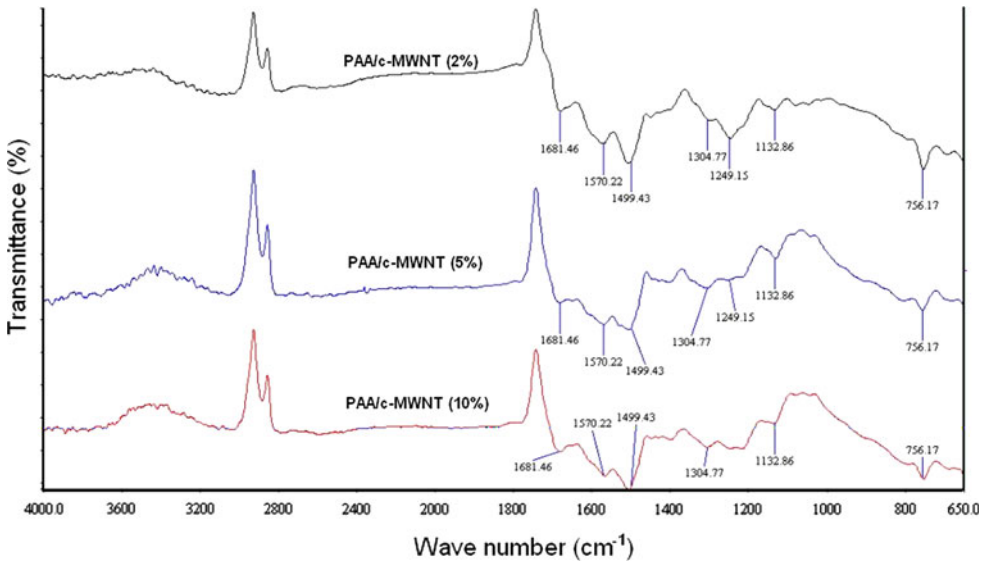

Fig. 5 FT-IR of PAA/c-MWNTs

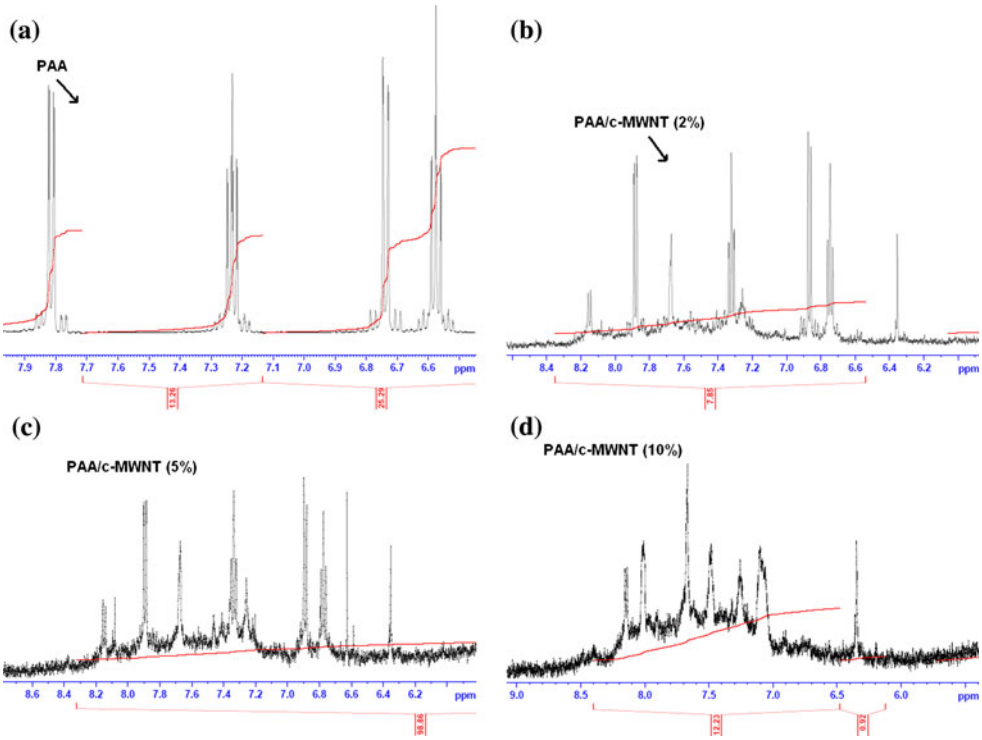

Fig. 6 NMR spectra of **a** bare PAA; **b** PAA/c-MWNT (2%); **c** PAA/c-MWNT (5%); **d** PAA/c-MWNT (10%)

copolymer content. From these observations, it can be attributed that the coating of copolymer takes place only at the outer surface of the c-MWNTs. The formation of the copolymer-coated tubular nanocomposite is believed to arise from the strong interaction between the co-monomer and c-MWNTs. This interaction is thought to be made up of two components: one is the π–π electron interaction between the MWNTs and the comonomer [47] and the other is the hydrogen bond interaction between the carboxyl groups of the c-MWNTs and amino groups of the co-monomers. Such a strong interaction ensures that the co-monomer molecules are adsorbed on the surface of the c-MWNTs. The polymerization of co-monomer inside the c-MWNTs is hindered by the restricted access of the reactants to the interior of the c-MWNTs because of the presence of the carboxyl group at the ortho position of the co-monomer. This is in agreement with the findings reported in the literature [48].

TEM

The TEM of 10% c-MWNT is presented in Fig. 8. From the figure, it can be concluded clearly that PAA/c-MWNTs composite fibrous phases have coaxially tubular structures. This PAA/c-MWNT composite is the typical core–shell

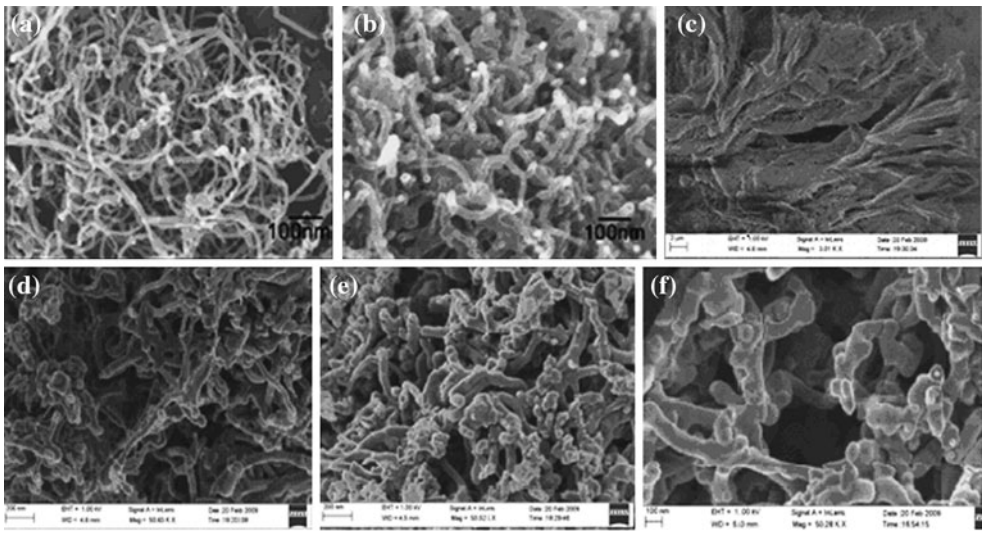

Fig. 7 SEM images of **a** MWCNT; **b** c-MWCNT; **c** bare anthranilic acid; **d** PAA/c-MWCNT (2%); **e** PAA/c-MWCNT (5%); **f** PAA/c-MWCNT (10%)

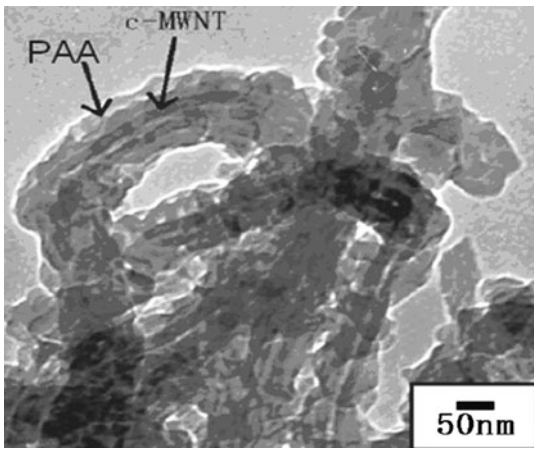

Fig. 8 TEM image of PAA/c-MWNT (10%)

structure, and the c-MWNT serves as the core and is dispersed individually into the PAA matrices.

XRD

The X-ray diffraction data for PAA and PAA/c-MWNT composites are shown in Fig. 9. For PAA, the X-ray scattering patterns exhibit amorphous structure while PAA/c-MWNT composites have relatively good crystalline structure. With the increasing of c-MWNTs, new diffraction peaks at $2\theta = 25.9°$ and 43° are attributed indicating c-MWNTs are as a core in the composites.

Conductivity

The electrical conductivities PAA/c-MWNT composites were measured using the standard Van Der Pauw DC four-probe method shown in Fig. 10. The conductivity of PAA synthesized in the presence of hydrochloric acid at room temperature is of 3×10^{-3} S/cm. Meanwhile, by the addition of 2 wt% c-MWNT into PAA, the conductivity at room temperature increases from 3 to 3.8×10^{-3} S/cm. Further, the conductivity at room temperature gradually increases to 5.6×10^{-4}, 9.8×10^{-3} S/cm for 5 and 10 wt% c-MWNT content. The reason for improvement in conductivity is the π–π^* interaction between the surface of c-MWNTs and the quinoid ring of the copolymer chain [49–51], which effectively improves the degree of electron

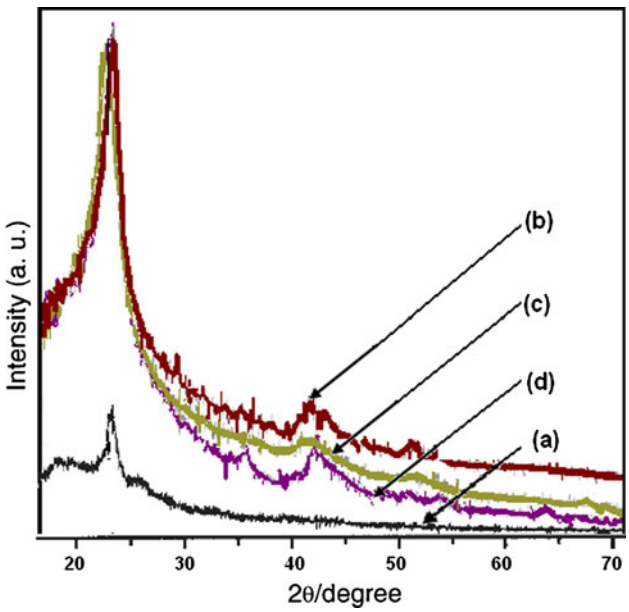

Fig. 9 X-ray diffraction data of *a* PAA/c-MWNT (0%); *b* PAA/c-MWNT (2%); *c* PAA/c-MWNT (5%); *d* PAA/c-MWNT (10%)

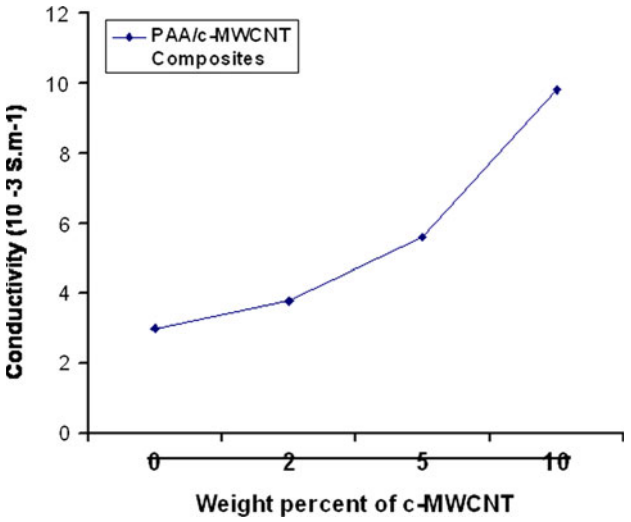

Fig. 10 Conductivity versus the weight percent of c-MWNT/PAA composites

delocalization between the two components, as confirmed by FT-IR and UV–visible and ^{1}H NMR spectra.

Conclusion

Poly(anthranilic acid) c-MWNTs nanocomposites were successfully synthesized via in situ polymerization. The nanocomposites were characterized using UV–visible, FT-IR, NMR, and XRD analysis. The interaction between c-MWNTs and copolymer chain was confirmed by FT-IR and UV–visible, and NMR spectra. The morphology of PAA/c-MWNT composites contains both the thinner fibrous phase and the larger block phase. It is assumed that c-MWNTs were used as a core in the formation of tubular shells of the fibrous PAA/c-MWNT composites. The highly ordered structures of nanocomposites were confirmed by XRD patterns. Room temperature conductivity of nanocomposite increased with the increase of c-MWNT.

Acknowledgements The authors are thankful to Dr. S. Sasmal, Central Rice Research Institute, Cuttack-753006, and Prof. M. C. Adhikary, Fakir Mohan University for their encouragements.

References

1. Iijima S (1991) Nature 354:56
2. Despres JF, Deguerre E, Lafdi K (1995) Carbon 33:87
3. Treacy MMJ, Ebbesen TW, Gibson JM (1996) Nature 381:678
4. Overney G, Zhong W, Tomanek D (1993) Z Phys D 27:93
5. Robertson DH, Brener DW, Mintmire JW (1992) Phys Rev B 45:12592
6. Chopra NG, Benedict LX, Crespi VH, Cohen ML, Louie SG, Zettl A (1995) Nature 377:135
7. Wagner HD, Lourie O, Feldman Y, Tenne R (1998) Appl Phys Lett 72:188
8. Iijima S, Brabec C, Maiti A, Bernholc J (1996) J Chem Phys 104:2089
9. Lourie O, Wagner HD (1998) J Mater Res 13:2418
10. Wong EW, Sheehan PE, Lieber CM (1997) Science 277:1971
11. Poncharal P, Wang ZL, Ugarte D, de Heer WA (1999) Science 283:1513
12. Meyyappan M (2005) Carbon nanotubes: science and applications. CRC Press, Boca Raton, FL
13. Salvetat JP, Andrew G, Briggs D, Bonard JM, Basca RR, Kulik AJ, Stöckli T, Burnham NA, Forró L (1999) Phys Rev Lett 82:944
14. Fan S, Chapline MG, Franklin NR, Tombler TW, Cassell AM, Dai H (1999) Science 283:512
15. Dai H, Hafner JH, Rinzler AG, Colbert DT, Smalley RE (1996) Nature 384:147
16. Frank S, Poncharal P, Wang ZL, de Heer WA (1998) Science 280:1744
17. Tans SJ, Verschueren ARM, Dekker C (1998) Nature 393:49
18. Ajayan PM, Stephan O, Colliex C, Trauth D (1994) Science 265:1212
19. Tang BZ, Xu HY (1999) Macromolecule 32:2569
20. Jin Z, Pramoda KP, Xu G, Goh SH (2001) Chem Phys Lett 337:43
21. Hwang GL, Hwang KC (2001) J Mater Chem 11:1722
22. Dong SR, Tu JP, Zhang XB (2001) Mater Sci Eng A Struct Mater Prop Microstruct Process 313:83
23. Jia ZJ, Wang ZY, Xu CL, Liang J, Wei BQ, Wu DH, Zhu SW (1999) Mater Sci Eng A 271:395
24. Barraza HJ, Pompeo F, O'Rear EA, Resasco DE (2002) Nano Lett 2:797
25. Gao M, Huang SM, Dai LM, Wallace G, Gao RP, Wang ZL (2000) Angew Chem Int Ed 39:3664
26. Ge JJ, Hou HQ, Li Q, Graham MJ, Greiner A, Reneker DH, Harris FW, Cheng SZD (2004) J Am Chem Soc 126:15754
27. Salalha W, Dror Y, Khalfin RL, Cohen Y, Yarin AL, Zussman E (2004) Langmuir 20:9852
28. Kong H, Gao C, Yan DY (2004) Macromolecules 37:4022
29. Qu LW, Lin Y, Hill DE, Zhou B, Wang W, Sun XF, Kitaygorodskiy A, Suarez M, Connell JW, Allard LF, Sun YP (2004) Macromolecules 37:6055
30. Ago H, Petritsch K, Shaffer MSP, Windle AH, Friend RH (1999) Adv Mater 11:1281
31. Kymakis E, Amaratunga GA (2002) Appl Phys Lett 80:112
32. Woo HS, Czerw R, Webster S, Carroll DL, Park JW, Lee JH (2001) Synth Met 116:369
33. MacDiarmid AG, Chiang JC, Richter AF (1987) Synth Met 18:285
34. Cao Y, Smith P, Heeger AJ (1992) Synth Met 48:91
35. Zhang XT, Zhang J, Wang RM, Liu ZF (2004) Carbon 42:1455
36. Long YZ, Chen JZ, Zhang XT, Zhang J, Liu ZF (2004) Appl Phys Lett 85:1796
37. Ramamurthy PC, Malshe AM, Harrell WR, Gregory RV, Mcguire K, Rao AM (2004) Solid State Electron 48:2019
38. Wei ZX, Wan MX, Lin T, Dai LM (2003) Adv Mater 15:136
39. Sainz R, Benito AM, Martinez MT, Galindo JF, Sotres J, Bar′o AM, Corraze B, Chauvet O, Maser WK (2005) Adv Mater 17:278
40. Wu TM, Lin YW, Liao CS (2005) Carbon 43:734
41. Nguyen MT, Diaz AF (1995) Macromolecules 28:3411
42. Yan H, Wang H-J, Adisasmito S, Toshima N (1996) Bull Chem Soc Jpn 69:2395
43. Malinauskas A (2004) J Power Sources 126:214
44. Dai L, Lu J, Matthews B, Mau WH (1998) J Phys Chem B 102:4049
45. Roy BC, Gupta MD, Ray JK (1995) Macromolecules 28:1727
46. Ramanathan T, Fisher FT, Ruoff RS, Brinson LC (2005) Chem Mater 17:1290

47. Star A, Stoddart JF, Steuerman D, Diehl M, Bouaki A, Wong EW, Yang X, Chung SW, Choi H, Heath JR (2001) Angew Chem Int Ed 40:1721
48. Deng M, Yang B, Hu Y (2005) J Mater Sci 40:5021. doi: 10.1007/s10853-005-1623-6
49. Jeevananda T, Siddaramaiah B, Kim NH, Heo SB, Lee JH (2008) Polym Adv Technol 19:1754
50. Cochet M, Maser WK, Benito AM, Callejas MA, Martinez MT, Benoit JM, Schreiber J, Chauevt O (2001) Chem Commun 27:1450. doi:10.1039/b104009j
51. Pearson DS, Pincus PA, Heffner GW, Dahman SJ (1993) Macromolecules 26:1570–1575